Phase Diagram of the 4D U(1) Lattice Pure Gauge Theory

Rafael Carreira de Jesus Torres[1]

[1] *CeFEMA, Instituto Superior Técnico, Universidade de Lisboa, Av. Rovisco Pais, 1049-001 Lisboa, Portugal*

Lattice gauge theory (LGT) provides a framework to understand confinement in gauge theories, which is fundamental in theories such as quantum chromodynamics. In $3\mathcal{D}$ U(1) LGT, confinement is present throughout all of the parameter space, while in $4\mathcal{D}$ a phase transition takes place between a confining phase and a Coulomb phase, in which the charges interact according to quantum electrodynamics. In this project, we simulate $4\mathcal{D}$ U(1) LGT using the Monte Carlo method, using the Polyakov loop and the string tension as the order parameters identifying the phase transition. Moreover, by using anisotropic lattices, we recover the critical coupling at which the transition occurs for different temperatures, and construct the phase diagram of this theory. We further investigate the order of the phase transition for isotropic lattices, finding a first order transition at low temperatures, which becomes weaker with increasing temperature, until in becomes second order.

Keywords: Lattice gauge theory, Phase transition, Phase diagram, Confinement, Monte Carlo.

I. INTRODUCTION

Lattice gauge theories (LGT) [1] allow for the study of gauge theories without using perturbative methods. Performing non-perturbative calculations on a gauge theory in continuous spacetime involves the evaluation of infinite dimensional path integrals, which is not computationally feasible. By Wick rotating spacetime into Eucledian space and discretizing spacetime onto a finite lattice, the path integral becomes finite dimensional which allows for the theory to be simulated and calculations to be made using stochastic techniques. Taking the lattice size to infinity and the lattice spacings to zero, the continuum theory is recovered.

In this work, we will be interested in the gauge theory which is symmetric under the compact U(1) group. In three dimensions, the compact U(1) lattice gauge theory exhibits confinment through all the parameter space, so that free charges can not be observed. The four dimensional U(1) LGT is even more interesting, as it also exhibits a confining phase at strong coupling, but, at weak coupling, charged particles interact through a Coulomb interaction, as in quantum electrodynamics (QED). At some coupling, a phase transition is observed separating the two phases of the theory. The goal of this work is to study the phases of the compact $4\mathcal{D}$ U(1) LGT, by simulating the theory and computing observables using Markov Chain Monte Carlo methods. By running simulations at different temperatures, we obtain a phase diagram of this theory at a full range of values for the temperature and coupling, indicating the nature of the phase transition, which is still missing from the literature.

We begin by introducing the topic of lattice gauge theory in section II, following [2, 3], where we construct the action for the pure U(1) LGT, and present observables relevant to this study. Then, in section III, we look into the strong and weak coupling limits of U(1) LGT, introduce the mechanism responsible for the phase transition, and discuss order parameters which allow the distinction between the two phases. Section IV is devoted to a presentation of the numerical methods used in the generation of configurations for the simulation of this theory. Finally, we present the results of this work in section V and conclude in section VI.

II. LATTICE GAUGE THEORY

Fermion Hamiltonian: The fermionic part of the Hamiltonian, before enforcing gauge invariance, is given by

$$H_F = \int \mathrm{d}^3 r \bar{\psi}(r) \left(i\gamma_\mu \partial_\mu + m\right) \psi(r) \,. \tag{1}$$

In order to write the fermionic Hamiltonian on the lattice, we need to discretize the field derivative, which can be done by approximating the derivative with a central difference, on a small interval $2a$, with a the lattice spacing, that is, $\partial_\mu \psi(r) \to \frac{1}{2a}(\psi(r+\hat{\mu}) - \psi(r-\hat{\mu}))$, where $\hat{\mu}$ denotes the unit vector in the μ direction. Replacing the derivative in the Hamiltonian by the central difference approximation, and discretizing the integral as $\int d^3 r \to a^3 \sum_{r\in\Lambda}$, we obtain the following Hamiltonian

$$H_F = a^3 \sum_{r\in\Lambda} \bar{\psi}(r) \left(\sum_{\mu=1}^{3} i\gamma_\mu \frac{\psi(r+\hat{\mu}) - \psi(r-\hat{\mu})}{2a} + m\psi(r) \right) . \tag{2}$$

Much like the in continuum case, we now need to impose gauge invariance on the discretized Hamiltonian. On the lattice, we implement the gauge transformations by choosing an element $\Omega(r)$ of the local symmetry group for each lattice site r, such that the fields transform as $\psi(r) \to \Omega(r)\psi(r)$ and $\bar{\psi}(r) \to \bar{\psi}(r)$. When applying this gauge transformation, we find that the mass term is left invariant, as in the continuum case, while the discretized derivative term is not. However, we can make this term invariant under this gauge transformation if we introduce a new field $U_\mu(r)$ in the Hamiltonian, between the two fermion fields, that transforms as

$$U_\mu(r) \to \Omega(r) U_\mu(r) \Omega(r+\hat{\mu})^\dagger \,. \tag{3}$$

Equation 3 shows that $U_\mu(r)$ transforms as an element of the symmetry group considered. Moreover, because of the way this field appears in the Hamiltonian, it can be viewed as belonging to the link connecting lattice sites r and $r+\hat{\mu}$ and being oriented in the μ direction, which is why these are refereed to as *link variables*. A representation of the link variable can be seen in figure 1

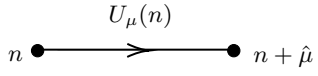

FIG. 1. The link variable $U_\mu(x)$ connecting lattice sites n and $n+\mu$.

Given that the link variables are oriented, we can also consider link variables in the opposite direction, connecting the lattice sites r and $r-\hat{\mu}$ defined as $U_{-\mu}(r) = U_\mu^\dagger(r-\hat{\mu})$, which transform as $U_{-\mu}(r) \to \Omega(r) U_{-\mu}(r) \Omega(r-\hat{\mu})^\dagger$.

Having defined the link variables and their transformation properties, we can now write the fermion Hamiltonian on the lattice as

$$H_F = a^3 \sum_{r\in\Lambda} \bar{\psi}(r) \left(\sum_{\mu=1}^{3} i\gamma_\mu \frac{U_\mu(r)\psi(r+\hat{\mu}) - U_{-\mu}(r)\psi(r-\hat{\mu})}{2a} + m\psi(r) \right) . \tag{4}$$

Gauge Field Hamiltonian: The lattice counterpart of the gauge fields are the link variables, $U_\mu(r) = \exp(igaA_\mu(r))$, where g is the gauge coupling and $A_\mu(r)$ is the gauge field. As such, in order to build the gauge field Hamiltonian, we need to construct a quantity composed by link variables, that is gauge invariant. Actually, in order to construct the counterpart of the continuum gauge field Hamiltonian, it is enough to use the *plaquette*[1], $\Pi_{\mu\nu}$, the shortest non-trivial closed path of link variables, shown in figure 2, defined as

$$\begin{aligned} \Pi_{\mu\nu}(r) &= U_\mu(r) U_\nu(r+\hat{\mu}) U_{-\mu}(r+\hat{\mu}+\hat{\nu}) U_{-\nu}(r+\hat{\nu}) \\ &= U_\mu(r) U_\nu(r+\hat{\mu}) U_\mu(r+\hat{\nu})^\dagger U_\nu(r)^\dagger . \end{aligned} \tag{5}$$

Since the link variables $U_\mu(r)$ commute with each other, such a term is not be enough to produce nontrivial dynamics. In general, link variables can rotate in the symmetry group considered, and as such, we can include in the Hamiltonian a term built from the operator $n_\mu(r)$ conjugate to $U_\mu(r)$ at each lattice link, written as[4] $\frac{1}{2}\sum_{r,\mu}(n_\mu(r))^2$. With these two terms, we can write the gauge field Hamiltonian as

$$H_G = \frac{U}{2} \sum_{r\in\Lambda} \sum_{\mu=1}^{3} (n_\mu(r))^2 - K \sum_{r\in\Lambda} \sum_{\substack{\mu,\nu=1 \\ \mu<\nu}}^{3} \mathrm{Re}\left[\mathrm{tr}\left(\Pi_{\mu\nu}(r)\right)\right] . \tag{6}$$

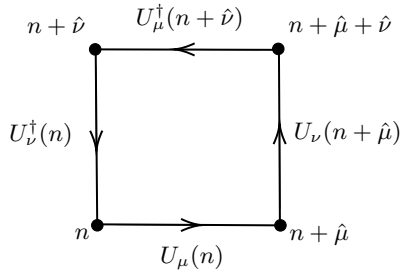

FIG. 2. The plaquette $\Pi_{\mu\nu}(n)$ is defined at each lattice site as the product of link variables $U_\mu(n)$ oriented around an elementary square.

Pure U(1) Lattice Gauge Theory: In this work, we will be interested in the case of the $U(1)$ lattice gauge theory, without fermions. For this symmetry group, the link variables $U_\mu(r)$ correspond to a complex number with a given phase, $U_\mu(r) = e^{i\phi_\mu(r)}$, so the plaquette becomes

$$\begin{aligned} \Pi_{\mu\nu}(r) &= U_\mu(r) U_\nu(r+\hat{\mu}) U_\mu^\dagger(r+\hat{\nu}) U_\nu^\dagger(r) \\ &= e^{i\phi_\mu(r) + \phi_\nu(r+\hat{\mu}) - \phi_\mu(r+\hat{\nu}) - \phi_\nu(r))} \\ &= e^{i(\Theta_{\mu\nu}(r)} , \end{aligned} \tag{7}$$

where $\Theta_{\mu\nu}(r)$ is the phase of the plaquette $\Pi_{\mu\nu}(r)$. Then, the Hamiltonian in equation 6 can be written as

$$H = \frac{U}{2} \sum_{r,\mu} (n_\mu(r))^2 - K \sum_{r,\mu<\nu} \cos\left[\Theta_{\mu\nu}(r)\right] . \tag{8}$$

The two terms of this Hamiltonian can be interpreted in analogy with the eletrodynamics Hamiltonian. The link variable $U_\mu(r)$ is given by $U_\mu(r) = \exp(igaA_\mu(r))$, so we have the relation $\phi_\mu(r) = gaA_\mu(r)$ between the phase $\phi_\mu(n)$ and the gauge field $A_\mu(n)$, which in U(1) is the electromagnetic four-potential. As such, in the continuum limit, performing a Taylor expansion on the second term, the sum over the spatial plaquettes becomes the square of the curl of the magnetic potential. Then, the second term of the Hamiltonian is the lattice form of the magnetic field squared. The operator $n_\mu(r)$, as the canonical momenta conjugated to $\phi_\mu(r)$, corresponds to the electric field flux through link $r+\hat{\mu}$, and as such, the first term of the Hamiltonian represents the electric field squared.

Derivation of the action: We now proceed to derive the action for the $U(1)$ lattice gauge theory, from the Hamiltonian in equation 8. The Hilbert space is spanned by the states $|\phi\rangle = \otimes_{r,\mu} |\phi_\mu(r)\rangle$ or $|n\rangle = \otimes_{r,\mu} |n_\mu(r)\rangle$ such that $e^{i\hat{\phi}_\mu(r)}|\phi\rangle = e^{i\phi_\mu(r)}|\phi\rangle$ and $\hat{n}_\mu(r)|n\rangle = n_\mu(r)|n\rangle$.

As the operator $\hat{n}_\mu(r)$ corresponds to the lattice version of the electric field flux through the link $r+\hat{\mu}$, the counterpart of the Gauss law on the lattice is that the charge, q, on a lattice site r is given by the sum of the electric flux through the links connected to site r, given by the $\hat{n}_\mu(r)$ operators as $\hat{Q}_r = \sum_\mu [\hat{n}_\mu(r) + \hat{n}_\mu(r-\hat{\mu})] = q$.

We are interested in studying the U(1) LGT without charges, so we consider the projector to this subspace of the Hilbert space, written as $P = \prod_r \delta_{\hat{Q}_r,0} = \int \prod_r \frac{d\theta(r)}{2\pi} e^{i\sum_r \hat{Q}_r\theta(r)}$, which has the properties $P^2 = P$ and $[P, H] = 0$. Thus, the partition function is given by $Z = \mathrm{tr}[e^{-\beta H} P]$.

In order to numerically simulate this theory, we perform a Trotter decomposition, by separating the partition function Z into N time intervals, with a temporal extent $\Delta\tau = \beta/N$. Up to terms of order $\Delta\tau$, we can then write the partition function as $Z = \mathrm{tr}\left[e^{-\beta H} P\right] = \mathrm{tr}\left[\left(e^{-\frac{\beta}{N} H} P\right)^N\right] = \int D\phi \prod_{\tau=0}^{N-1} \left\langle \phi_\tau \left| e^{-\Delta\tau H} P \right| \phi_{\tau+1} \right\rangle$, where $D\phi = \prod_{\tau=0}^{N-1} \sum_{r,l} \frac{d\phi_\mu(\tau,r)}{2\pi}$. Separating the Hamiltonian into the parts containing operators $\hat{\phi}$ and $\hat{n}$, as $H = H_{\hat{n}} + H_{\hat{\phi}}$ and introducing a partition of the identity in $|n\rangle$, we have

$$\begin{aligned} Z &= \int D\phi \prod_{\tau=0}^{N-1} \langle\phi_\tau| e^{-\Delta\tau H_{\hat{\phi}}} e^{-\Delta\tau H_{\hat{n}}} P |\phi_{\tau+1}\rangle + O(\Delta\tau) \\ &\simeq \int D\phi \sum_n \prod_{\tau=0}^{N-1} \langle\phi_\tau| e^{-\Delta\tau H_{\hat{\phi}}} |n_\tau\rangle \langle n_\tau| e^{-\Delta\tau H_{\hat{n}}} P |\phi_{\tau+1}\rangle \\ &= \int D\phi D\theta \sum_n \prod_{\tau=0}^{N-1} \langle\phi_\tau| e^{-\Delta\tau H_{\hat{\phi}}} |n_\tau\rangle \langle n_\tau| e^{-\Delta\tau H_{\hat{n}}} e^{i\sum_r \hat{Q}_r\theta(\tau,r)} |\phi_{\tau+1}\rangle \\ &= \int D\phi D\theta \sum_n \prod_{\tau=0}^{N-1} \langle\phi_\tau| e^{-\Delta\tau H_{\hat{\phi}}} |n_\tau\rangle \langle n_\tau| e^{-\Delta\tau H_{\hat{n}}} e^{i\sum_{r,\mu}[\hat{n}_\mu(\tau,r) + \hat{n}_{\tau,\mu}(r-\hat{\mu})]\theta(\tau,r)} |\phi_{\tau+1}\rangle , \end{aligned} \tag{9}$$

where the sum in n in given by $\sum_n = \prod_{\tau=0}^{N-1} \prod_{r,\mu} \sum_{n_\mu(\tau,r)}$ and we introduced the definition of the projector P with $D\theta = \prod_{\tau=0}^{N-1} \prod_r \frac{d\theta(\tau,r)}{2\pi}$ in the third line. In the last step, we used the Gauss law. Then, by acting with the $\hat{\phi}$ and $\hat{n}$ operators on $\langle\phi_\tau|$ and on $\langle n_\tau|$, respectively, using $\langle \phi \mid n \rangle = \exp(i\sum_{r\mu} \phi_\mu(r) n_\mu(r))$ and noting that $\sum_{r,\mu}[n_\mu(\tau,r) + n_\mu(\tau,r-\hat{\mu})]\theta(\tau,r) = \sum_{r,\mu} n_\mu(\tau,r)[\theta(\tau,r) + \theta(\tau,r+\hat{\mu})]$, we finally obtain a partition function of the form $Z = \int D\phi D\theta \sum_n e^{-S[\phi,\theta,n]}$ with

$$\begin{aligned} S[\phi,\theta,n] = &- \Delta\tau K \sum_{\tau,r,\mu<\nu} \cos\left[\phi_\mu(\tau,r) - \phi_\nu(\tau,r+\hat{\mu}) + \phi_\mu(\tau,r+\hat{\nu}) - \phi_\nu(\tau,r)\right] \\ &- i \sum_{\tau,r,\mu} \left[\phi_\mu(\tau,r) - \phi_\mu(\tau+1,r) + \theta(\tau,r) + \theta(\tau,r+\hat{\mu})\right] n_\mu(\tau,r) \\ &+ \Delta\tau \frac{U}{2} \sum_{\tau,r,\mu} \left[n_\mu(\tau,r)\right]^2 . \end{aligned} \tag{10}$$

In order to identify this action with a theory on a (3+1)$\mathcal{D}$ lattice, we identify $\hat{\theta}(\tau, r)$ with the phase of a link variable in the temporal direction, $\phi_0(\tau, r)$, so that the the second term in equation 10 corresponds to the phase of a space-time plaquette.

We can then approximate the sum in n in the partition function in equation 10 for $\Delta\tau U \gg 1$ using the Villain approximation[5], given by

$$e^{z\cos(\Phi)} = \sum_n I_n(z) e^{in\Phi} \simeq \sum_n e^{-\frac{1}{2z}n^2 + i\Phi n}\,, \tag{11}$$

which is valid for $z \gg 1$. Then, we obtain the approximated partition function, given by $Z = \int D\phi e^{-S[\phi]}$ with the action $S[\phi]$ given by

$$\begin{aligned} S[\phi] = &-\Delta\tau K \sum_{n,\mu<\nu} \cos\left[\phi_\mu(n) + \phi_\nu(n+\hat{\mu}) - \phi_\mu(n+\hat{\nu}) - \phi_\nu(n)\right] \\ &- \frac{1}{\Delta\tau U} \sum_{n,\mu} \cos\left[\phi_\mu(n) + \phi_0(n+\hat{\mu}) - \phi_\mu(n+\hat{e}_0) - \phi_0(n)\right]\,, \end{aligned} \tag{12}$$

where we relabeled the spacetime coordinates as $n = (\tau, r)$ with directions $\mu, \nu = (0, 1, 2, 3)$ with $\mu = 0$ for the temporal direction.

This is the canonical action for the U(1) lattice gauge theory. In simulations of lattice gauge theory, it is usual to set the coupling of the spatial and space-time parts of the action equal, as $\Delta\tau K = \frac{1}{\Delta\tau U} = \beta$, and write the action for the *isotropic* U(1) lattice gauge theory as

$$S[\phi] = -\beta \textstyle\sum_{n,\mu<\nu} \cos\left[\phi_\mu(n) + \phi_\nu(n+\hat{\mu}) - \phi_\mu(n+\hat{\nu}) - \phi_\nu(n)\right]\,, \tag{13}$$

where β is the *coupling parameter*. Alternatively, we can treat spatial and temporal lattice directions differently, by introducing an *anisotropy parameter* ξ in the action, and write it as [6]

$$\begin{aligned} S[\phi] = &-\frac{\beta}{\xi} \sum_{n,\mu<\nu} \cos\left[\phi_\mu(n) + \phi_\nu(n+\hat{\mu}) - \phi_\mu(n+\hat{\nu}) - \phi_\nu(n)\right] \\ &- \beta\xi \sum_{n,\mu} \cos\left[\phi_\mu(n) + \phi_0(n+\hat{\mu}) - \phi_\mu(n+\hat{e}_0) - \phi_0(n)\right]\,. \end{aligned} \tag{14}$$

Observables: The ultimate goal of discretizing the continuum gauge theory to a lattice was to make it finite and computable. Having defined the partition function for the U(1) pure gauge theory in the lattice, we can now compute observables. The average value of an observable $\hat{O}$ on the lattice is given by

$$\langle \hat{O} \rangle = \frac{1}{Z} \int \mathrm{e}^{-S[U]} O[U] \mathcal{D}[U]\,, \tag{15}$$

where $O[U]$ is a gauge invariant functional of lattice links U obeying $O[U] = O\left[\Omega U \Omega^\dagger\right] = O\left[U'\right]$. As we have seen when constructing the gauge field Hamiltonian, such a quantity is the trace of an ordered product of link variables across a closed loop. Indeed these traced loops of link variables can be used to construct observables on the lattice. One example is the plaquette, $U_{\mu\nu}$, defined in equation 5.

Another observable we will be considering is the *Wilson loop*, defined as the trace of a product of link variables around a closed loop, $\mathcal{L}$, over one spatial direction and one temporal direction as $W_\mathcal{L}[U] = \mathrm{tr}\left[\prod_{(n,\mu)\in\mathcal{L}} U_\mu(n)\right]$

Taking advantage of the periodic boundary conditions, we can also consider the trace of the product of temporal link variables over the full extent of the lattice on a point on the spatial lattice, and define the *Polyakov loop* as $P(r) = \mathrm{tr}\left[\prod_{j=0}^{N_T-1} U_0(r, j)\right]$

We can relate the Wilson loop extending over a distance r in the spatial direction and n_t in the temporal direction to the potential between a static fermion-antifermion pair, $V(r)$ as

$$\langle W_\mathcal{L}[U] \rangle \propto e^{-n_t a V(r)} (1 + \mathcal{O}(e^{-n_t a \Delta E}))\,, \tag{16}$$

where $V(r)$ denotes the potential and $\Delta E = E_2 - E_1$ is the energy difference between the fermion-antifermion pair and its first exited level. In the limit of large n_t, i.e., for Wilson loops extending over large temporal distances, we can neglect the $\mathcal{O}(e^{-n_t a \Delta E})$ terms and use the Wilson loop to calculate the potential.

Similarly, since considering the Wilson loop over the full extent of the temporal direction reduces it to the product of two Polyakov loops in opposite directions, one at the spatial position r_1 and the other at r_2, we can also relate the potential to the *Polyakov loop correlator* as

$$\langle P(r_1) P^\dagger(r_2) \rangle \propto e^{-N_t a V(r)} (1 + \mathcal{O}(e^{-N_t a \Delta E}))\,. \tag{17}$$

Temperature: Since we want to study the phases of this theory at different temperatures, we need a way to control the temperature of the system. In order to do this, we take advantage of the analogy between the partition function given in terms of the euclidean path integral formulation, and the partition function given in terms of the canonical ensamble of statistical physics. From the path integral formulation we have $Z = \mathrm{tr}\left[e^{-T_E H}\right]$ where T_E denotes the extent in the euclidean time direction and H the Hamiltonian. From statistical physics, we have that the partition function in given by $Z = \mathrm{tr}\left[e^{-\beta H}\right]$ where $\beta = 1/Tk_B$, with T the temperature and k_B the Boltzmann factor.

By matching the two definitions of the partition function, we can identify β with the lattice temporal temporal extent, $\beta = T_E$. On the lattice, the temporal extent is given by the product of the temporal lattice spacing with the number of points in the temporal direction, $T_E = a_t N_t$. Setting $k_B = 1$, we find that the temperature is related to the temporal lattice spacing and the lattice time extent as

$$\frac{1}{T} = a_t N_t \Leftrightarrow T = \frac{1}{a_t N_t}\,. \tag{18}$$

III. U(1) LATTICE GAUGE THEORY

Strong Coupling Limit: In the strong coupling limit, $U \gg K$, the Hamiltonian in equation 8 can be written as

$$H_0 = \frac{U}{2} \sum_{r,\mu} \left(n_\mu(r)\right)^2\,. \tag{19}$$

The ground state corresponds to having $n_\mu(r) = 0$ at all lattice links. Excited states of this Hamiltonian correspond to taking $n_\mu(r) \neq 0$ in links forming closed loops on the lattice, respecting $\sum_\mu \left[\hat{n}_\mu(r) + \hat{n}_\mu(r - \hat{\mu})\right] = 0$. The energy of each state depends on the number of $n_\mu(r) \neq 0$, and as such, it is proportional to the length of the loop.

Taking the potential term in equation 8 into account, the loop acquires quasimomentum, and can also move trough the lattice. Another effect arising from considering the cosine term in the Hamiltonian is that this term can generate new loops, which alter the shape of the initial loop, and as such the state becomes a superposition of closed loops with different shapes. [7]

Physically, $n_\mu(r)$ corresponds to the electric flux through the link $r+\mu$. As such, these closed loops correspond to flux lines. If we introduce two charges at two lattice sites, an electric flux line is generated between them. Since in this limit the energy of a state is proportional to the length of the flux lines, the energy of this state will be proportional to the distance between the charges, and as such, the system is said to be in the *confined phase*. In fact, this is the case also for non-abelian theories. Both abelian and non-abelian theories in the strong coupling regime exhibit linear confinement. [1]

Weak Coupling Limit: In three dimensional lattice gauge theory, we have a partition given by in equation 13. In the weak coupling limit, we can Taylor expand the action around one well of the cosine. Then, in order to restore the periodicity of the action, we can add an integer $n_{\mu\nu}(x)$, which is defined on the plaquette, so that the action can be written as

$$Z = \sum_{n_{\mu\nu}(x)} \int D\phi \exp\left(-\beta \sum_{n,\mu<\nu} \left(\Theta_{\mu\nu} + 2\pi n_{\mu\nu}(x)\right)^2\right), \tag{20}$$

with $n_{\mu\nu}(x)$ such that $\Theta_{\mu\nu} + 2\pi n_{\mu\nu}(x)$ is in the interval $[\pi, \pi]$. As we saw in the previous section, $\Theta_{\mu\nu}$ is the lattice counterpart of the magnetic flux. As such, $n_{\mu\nu}(x)$ can be seen as a flux appearing due to the passage of a string through a plaquette. A string entering a cube through a plaquette, can either go out of the cube through another plaquette or have its endpoint inside the cube. In order for the flux to be conserved, if the string has its endpoint in a cube centered at x^*, the flux going into the cube must dissipate through its six faces. This is identified as a monopole. [8] As such, by summing the $n_{\mu\nu}(x)$ variables around a cube, we can obtain the monopole charge, defined as $q_{x^*} = \sum_{cube} n_{\mu\nu}(x)$. Using this variable, we can write the partition function as a partition function for the free photons multiplied by a partition function for the monopoles, as [7]

$$Z = \prod_x \int D\phi \exp\left(-\frac{\beta}{2}\sum_{x,\delta}(\Pi_{\mu\nu})^2\right) \sum_{q_{x^*}} \exp\left(-\frac{\beta}{2}\sum_{x^*,x^{*\prime}} \Delta^{-1}_{xx^*_*} q_{x^*} q_{x^*} 2\pi^2\right), \tag{21}$$

where $\Delta^{-1}_{xx'_*}$ is the inverse lattice Laplace operator, and so the monopoles behave like charges interacting through the Coulomb potential. In the large β limit, the monopoles are combined into neutral dipoles, formed by a monopole and an antimonopole connected by a string. How this leads to confinement of electric charges can be understood through an analogy with a type II superconductor in a external magnetic field. If the external magnetic field penetrates the superconductor, the particles in the vacuum, i.e., the electrons of the superconductor, establish electric currents which confine the magnetic field to a one dimensional flux tube. Similarly, in the U(1) gauge system at weak coupling, if a pair of electric charges is introduced in the vacuum, the vacuum particles, which in this case are the magnetic monopoles, establish magnetic currents which confine the electric field between the charges to a flux tube, which has constant energy, and thus leads to a linear potential, which corresponds to confinement. [9]

In the previous section, we saw that in the strong coupling limit, U(1) LGT was in the confined phase, with a potential between two charges depending linearly on the distance between them. For the 2 + 1 dimensional case, we found a similar situation in the opposite limit. As such, $(2+1)\mathcal{D}$ U(1) LGT is expected to remain in the phase where electric charges are confined through all the parameter space. [10]

As we consider the theory in four dimensions, the instanton solutions of the $3\mathcal{D}$ case identified as monopoles, which were point like, can now move in a fourth direction, and so, in $4\mathcal{D}$ they are manifested as a current and can be represented by a world line [7]. In order for the magnetic flux to be conserved, these lines have to extend to infinity or to form closed loops on the lattice. As in the $3\mathcal{D}$ case, we can separate the partition function for this system into a partition function for the loops of magnetic flux lines, and a partition function for free photons. In the weak coupling limit, $\beta \gg 1$, the closed loops of magnetic flux represent the world lines of the monopole-antimonopole pairs that appeared in $3\mathcal{D}$ at this limit. The contribution of such a loop to the action is proportional to its length and, as such, in the infrared limit, the magnetic flux lines have no influence on the system which can thus be described only by the free photons. As such, in this limit, the energy spectrum has no mass gap, and our theory can be described by massless photons.

In the strong coupling limit, we found that this system was in the confined phase. However, in the weak coupling limit in four dimensions, we expect charges to interact according to QED, with the potential between two electric charges being of the Coulomb form, instead of linear. Therefore, for some critical value of the coupling parameter, β_c, we expect to find a phase transition such that for $\beta < \beta_c$ the system is in the confined phase and for $\beta > \beta_c$ the system is in the *Coulomb phase*. [11, 12]

Phase Transition: The distinguishing feature between the confining and non-confining phases is the potential, which should grow linearly with distance in the former case and should be of the Coulomb form in the latter. As such, we can distinguish between these two phases by calculating the potential, through the Polyakov loop correlator, according to equation 17. According to the form of the potential in the two phases, we can parameterize it as [2] $aV(r) = A + \frac{B}{r} + \sigma r$, where the first term is an irrelevant normalization to the energy, the second term is the Coulomb potential with strength B, and the last term is the linearly growing confining potential, with σ the *string tension*.

For large distances, the term σr dominates the potential. As such, if $\sigma \neq 0$, we have a linearly rising potential, corresponding to the confining phase. Only for $\sigma = 0$ do we have a Coulomb potential at large distances. Therefore, the string tension σ is an order parameter of our theory, distinguishing between the confining and non-confining phase.

At large distances, $a|r_1 - r_2| \to \infty$, we can factorize the Polyakov loop correlator in equation 17 as

$$\lim_{a|r_1-r_2|\to\infty} \left\langle P(r_1)P(r_2)^\dagger \right\rangle = \langle P(r_1)\rangle \left\langle P(r_2)^\dagger \right\rangle = |\langle P\rangle|^2, \tag{22}$$

where in the last step, we replaced the expectation value of the Polyakov loop at a given position with the spatial average of this quantity, since the average value must be translational invariant. In this limit, the potential in the confining phase goes to infinity, while in the Coulomb phase, it approaches a constant value. Taking this into account and inserting the result of equation 22 into the definition of the Polyakov loop correlator in equation 17 at large distances, we note that, due to the linear growth of the potential, the Polyakov loop should have a zero expectation value, $\langle P\rangle = 0$ in the confined phase, while in the Coulomb phase, it should have a finite value, $\langle P\rangle \neq 0$. As such, the Polyakov loop is also an order parameter which allows us

to distinguish between the two phases of the U(1) LGT.

IV. MARKOV CHAIN MONTE CARLO

Monte Carlo method: Physical systems usually have rather large phase spaces, which renders exact calculations impossible. One way to overcome this issue, is to consider the system's statistical behaviour, instead of trying to obtain analytical results. In lattice gauge theory, the expectation value of some observable is given by the functional integral $\langle O\rangle = \frac{1}{Z}\int \mathcal{D}[U]\mathrm{e}^{-S_G[U]}O[U]$ with $Z = \int \mathcal{D}[U]\mathrm{e}^{-S_G[U]}$, as explained in the previous section. For large lattice sizes, this integral becomes impossible to evaluate analytically. As such, we can consider an estimator of the expectation value, $\langle O\rangle$, by sampling N states (configurations) of the lattice, U_n, computing the value of the observable O in each configuration, and considering the sample mean $\langle O\rangle \approx \bar{O} = \frac{1}{N}\sum_{U_n} O\,[U_n]$, where the sum runs over configurations U_n distributed according to the Boltzmann probability distribution, $\exp(-S[U_n])$, and which has a variance $\sigma^2 = \langle(O - \langle O\rangle)^2\rangle$, which we can estimate as $s^2 = \frac{1}{N-1}\sum_{U_n}(O[U_n] - \bar{O})^2$.

Therefore, provided we are able to sample a set of configurations according to the desired probability distribution, we can obtain an estimate of the expectation value of observables, with an error $\epsilon = \sqrt{s^2/N}$.

Metropolis-Hastings Algorithm: The Metropolis-hasting algorithm [13, 14] is Markov chain Monte Carlo method for generating sequential configurations with a desired target distribution. This method provides a transition matrix that respects the detailed balance condition, necessary for the Markov Chain to evolve to an equilibrium distribution [15], after which we can generate equilibrium configurations.

In LGT, the variables of interest are the links on a $(3+1)$D lattice with periodic boundary conditions. We want to generate configurations with a target probability distribution proportional to the Boltzmann probability distribution, $e^{-S_G[U]}$, where $S_G[U]$ is the lattice gauge action defined in equation 13.

In U(1) LGT, the link variables are given by $U_n = e^{i\phi_n}$, so the configurations are defined by the link angles ϕ_n. As such, the algorithm for implementing the Metropolis-Hastings method for U(1) LGT consists in, for each link:

1. Generating a new value for the link angle, ϕ_n' according to a uniform random distribution;
2. Calculate the new value of the action, $S_G[U']$ with the proposed value for the new link variable;
3. Accept the new value for the link variable with a probability $P_{accept} = \min\left(1, \frac{e^{-S_G[U']}}{e^{-S_G[U]}}\right)$
4. If the new link variable is accepted, it replaces the old one. If not, the value of the link variable remains the same and we move one to the next iteration. Markov-time is incremented in any case.

We can now use this method to generate several configurations in order to calculate the estimator of the average values of the observables considered. In order to do this calculation, the configurations considered must be taken after the equilibrium probability distribution is reached. This calculation also assumes that the configurations considered are uncorrelated, which is not the case for configurations generated with a Markov chain. As such, we discard the first 2000 configurations, to ensure that calculations are done after the system thermalizes. Furthermore, we calculate the autocorrelation time between different configurations, τ, and only keep configurations separated by 3τ for the calculation of average values of observables.

V. SIMULATING THE U(1) LGT

A. Isotropic lattice

Average Plaquette: We simulate the action in equation 13 for different values of β and calculate the average plaquette, $W = \frac{1}{6N_tN_s^3}\sum_{n,\mu<\nu} Re\Pi_{\mu\nu}(n)$, as well as its susceptibility, $C_v = N_tN_s^3(\langle W^2\rangle - \langle W\rangle^2)$ for each of these values. We repeat this procedure for different extents of the lattice in the temporal direction, N_t, in order to study the theory at different temperatures, $T = \frac{1}{a_tN_t}$, while keeping the spatial extent fixed at $N_s = 24$. The results obtained can be seen in figure 3. In figure 3 (a), instead of plotting the average plaquette, W, we plot $1 - W$, in order to match the literature.

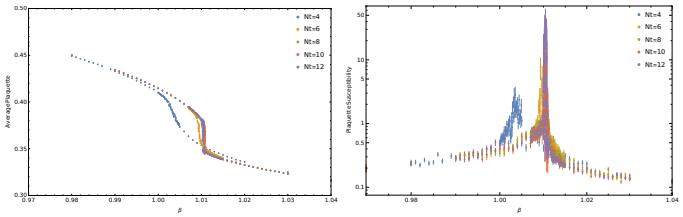

FIG. 3. Average value of the plaquette (a) and plaquette susceptibility (b) as a function of β for $N_t = 4, 6, 8, 10, 12$.

In figure 3 (a), we can see that the average plaquette undergoes a phase transition as we vary the value of the coupling parameter, β, which becomes evident in figure 3 (b) where we notice the peaks in the plaquette susceptibility. However, a quantity more suited to identify the phase transition, as we saw in section III is the Polyakov loop, at which we will be looking in the following.

Average Polyakov loop: The average Polyakov loop, $P = \frac{1}{N_s^3}\sum_r P(r)$ is determined in a similar way to the average plaquette, by simulating the action for different values of β and N_t, with $N_s = 24$. The average value of the Polyakov loop is shown in figure 4, where it can be seen that the Polyakov varies from $\langle P\rangle = 0$ for strong coupling to a finite value at weak coupling, denoting the transition from the confined to the deconfined phase. The precise value of the critical coupling, β_c, at which this phase transition occurs for each value of N_t can be obtained by determining the position of the peaks in the Polyakov loop susceptibility, $\chi_P = N_tN_s^3(\langle P^2\rangle - \langle P\rangle^2)$ shown in figure 4.

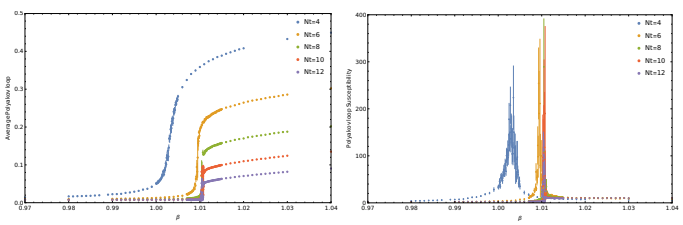

FIG. 4. Average value of the Polyakov loop (a) and Polyakov loop susceptibility (b) as a function of β for $N_t = 4, 6, 8, 10, 12$.

Phase diagram: In order to determine the value of the coupling, β_c, at which the phase transition occurs, the data for the Polyakov loop susceptibility close to the peak was

fitted to a Lorentzian function, for each value of N_t. In figure 5 we present the values of the critical coupling for each value of N_t plotted in the parameter space. It can be seen that the value of β_c increases with N_t, varying less for larger values of N_t, as we reach the limit of zero temperature. The results obtained are compatible with previous phase diagrams obtained in the literature [16], which validated our approach to determine the points at which the phase transition takes place, as well as the numerical simulations made.

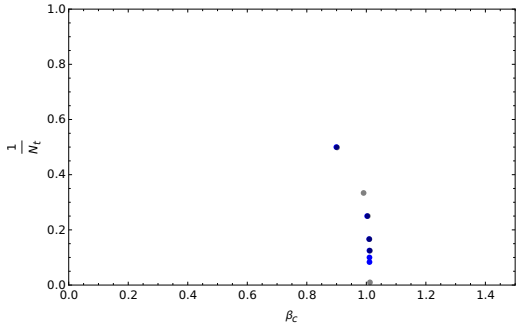

FIG. 5. Position of the peaks in the Polyakov loop susceptibility obtained in blue. In gray, the points from the phase diagram obtained in [16]. The results obtained show great agreement with the literature.

This phase diagram is incomplete, as we were only able to probe a narrow region of the parameter space by studying the isotropic lattice. In order to obtain a complete phase diagram, we need to consider the anisotropic lattice regularization. As will be seen in the next section, this regularization allows the study of the U(1) LGT at higher temperatures.

Potential: Another way to investigate the phase transition of the U(1) LGT is to look at the potential between two static charges, as seen in section III. Inverting the relation in equation 17, we can determine the potential at a given distance r, by calculating the average value of the correlator of two Polyakov loops separated by that distance, as

$$aV(r) = -\frac{1}{N_t}\log(< P(0)P^{\dagger}(r) >) \tag{23}$$

It is difficult to get significant statistics to calculate this correlator, as there are fluctuations in the value of the Polyakov loop, which lead to large statistical errors. In order to overcome this, we used the multihit [17, 18] and multilevel [19] methods to calculate the potential.

We calculated the potential for several values of β and found that for strong coupling (small β), the potential depends linearly with the distance r at large distances, showing that electric charges are confined in this region of the parameter space. For weak coupling (large β), we found a Coulomb potential, which shows that electric charges are no longer confined, and instead we have a situation similar to electrodynamics. In figure 6 we show the potential computed at two values of β, illustrating the two situations.

We fitted our results with a function of the form $aV(r) = A - \frac{b}{r} + \sigma r$, in order to determine the string tension, σ. In figure 7, we can see the value of the string tension decreasing near the phase transition, until it becomes zero in the Coulomb phase.

Order of the Phase Transition: When working very close to the phase transition, the lattice configurations generated by the Markov chain may oscillate between the two phases of the theory. Therefore, at values of the gauge coupling, β, near the phase transition, the absolute value of

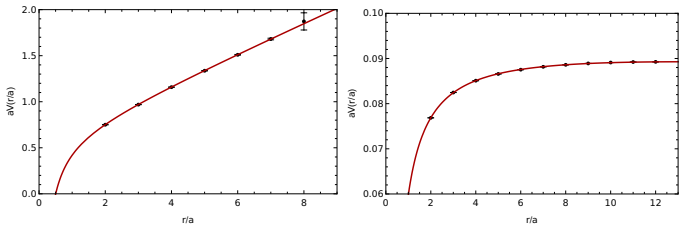

FIG. 6. Potential calculated on an isotropic 24^4 lattice for $\beta = 1, 3$, using the multihit and the multilevel methods. For $\beta = 1$, we obtain a linear potential at large distances, corresponding to the confined phase, while for $\beta = 3$ we obtain a Coulomb potential, approaching a constant value for large distances, characteristic of the deconfined phase.

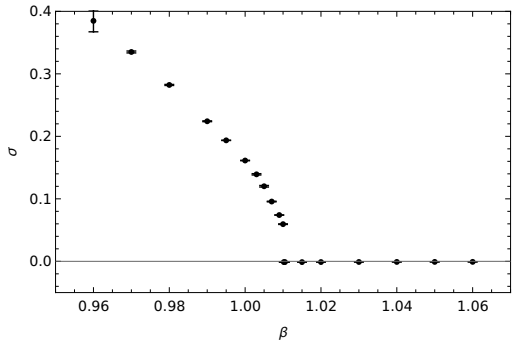

FIG. 7. String tension calculated for values of β near the phase transition. Before the phase transition, in the confined phase, this parameter has a finite value, and it decreases as we approach the phase transition, becoming zero in the deconfined phase.

Polyakov loop calculated on the configurations generated can be zero, $|P| = 0$, or a finite value, $|P| \neq 0$.If the transition is discontinuous, the value of the average Polyakov loop has a jump at the phase transition, and as such the value of the Polyakov loop calculated in configurations in the Coulomb phase can be significantly different from zero. These oscillations of the Markov chain between the two configurations introduce errors in obtaining the value of the average Polyakov loop very close to the phase transition. However, these also present a way to determine the order of the phase transition.

If the transition is discontinuous, by generating successive configurations near the phase transition with the Markov chain Monte Carlo method described in section IV, we expect to find values of the Polyakov loop for each configuration both at zero, and at a value away from zero. Then, by plotting an histogram of the absolute value of the Polyakov loop, we will find two peaks at the two values of the Polyakov loop for each phase, if the transition is of first order. By generating configurations at values of β near the phase transition, we found this two peak structure at large values of N_s for $N_t \geq 6$, indicating that, for isotropic lattices with these temporal extents, the transition is first order, as expected [20]. As an example, in figure 8 we present the histogram obtained for a simulation with $N_t = 8$, where we can see the double peak appearing at the phase transition.

For lattices with less points in the temporal direction, the two peak structure was not found. In particular for $N_t = 2$, as can be seen in figure 8, only one peak is seen at the phase transition. As we vary β from the confined phase to the Coulomb phase, in this case, we always have one peak, which is centered at larger values of the Polyakov loop, as β increases. As such, for the isotropic lattice with

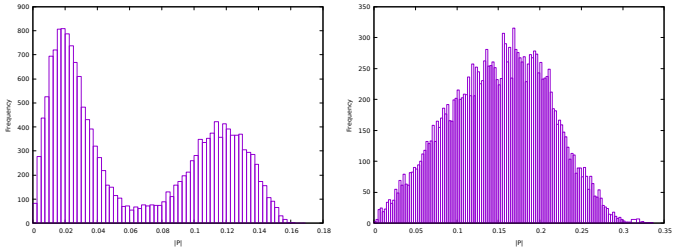

FIG. 8. Histogram of the absolute value of the Polyakov loop calculated in a four dimensional lattice with $N_s = 24$ for (a)$N_t = 8$ and (b)$N_t = 2$, at the value of the coupling parameter determined for the phase transition. For $N_t = 8$ at $\beta = 1.01043$, we can identify two peaks, indicating a first order transition. For $N_t = 2$ at $\beta = 0.89929$, only one peak is seen, indicating a continuous transition.

this extent of the temporal direction, we can identify the phase transition as continuous.

The situation for lattices with $N_t = 4$ was more complicated, as for smaller values of the spatial extent of the lattice, N_s, the theory appeared to have a weakly first order transition, with two peaks appearing in the Polyakov loop histogram very close to each other, with a significant overlap. However, as we increased N_s, the second peak becomes smaller and harder to identify. It is not clear whether the second peak is still present at large values of N_s, but because of the proximity between the two peaks, the smaller peak is harder to identify or if this peak vanishes at large spatial extents. As such, for $N_t = 4$, as we take the spatial size to infinity, the phase transition is either second order or very weakly first order.

These results agree with the literature [20], indicating a first order phase transition for $N_t \geq 6$ and a second order phase transition for $N_t = 2.$, as we approach the limit $N_t = 1$, where we recover the three dimensional XY model. A more clear picture of what happens for $N_t = 4$ could be obtained by investigating the scaling of the maximum value of the plaquette susceptibility, C_v with the spatial extent of the lattice, N_s. By determining the critical exponents of this quantity, it would be possible to confidently determine the order of the phase transitions.

B. Anisotropic lattice

In order to study this theory at different temperatures, we consider the anisotropic lattice regularization [6], by writting the action as in equation 14.

Since the anisotropy parameter gives a measure of the ratio between the spatial and temporal lattice spacings, $\xi = as/at$, by choosing different values of ξ, we can change a_t while keeping a_s constant, thus changing the temperature, given by $T = \frac{1}{N_t a_t} = \frac{\xi}{N_t a_s}$. Since in the isotropic case, we had the same lattice spacing a on all directions, by keeping the spatial lattice distance constant, we can express the temperature as $T = \frac{\xi}{N_t a}$, where a is the lattice spacing on the isotropic lattice.

As such, studying an anisotropic lattice with an anisotropy parameter ξ and N_t points in the time direction is equivalent to studying the isotropic lattice with $\frac{N_t}{\xi}$ points in the time direction, which allows us to probe new regions of the parameter space that were inaccessible through the isotropic regularization, and thus construct a more complete phase diagram of the $U(1)$ LGT. The simulations with the anisotropic lattice were conducted in the same way as for the isotropic lattice.

Phase diagram: In order to plot the phase diagram in terms of the parameters in the Hamiltonian model, we compare the anisotropic action used in the simulations, in equation 14 to the action derived from the Hamiltonian in section II, written in equation 12. By matching the coefficients multiplying the spatial and space-time parts of the actions in equations 14 and 12, and noting that the intervals $\Delta\tau$ used in the Trotter decomposition coincide with the lattice spacing in the temporal direction when we identify our theory with a $4\mathcal{D}$ LGT in section II, so that we can write the temperature as $T = \frac{1}{N_t \Delta\tau}$ we find the following relations between the simulation parameters and the Hamiltonian parameters

$$\frac{K}{U} = \beta^2 \quad , \quad \frac{T}{U} = \frac{\beta\xi}{N_t} . \tag{24}$$

Having determined the critical value of the coupling, β_c, for different values of N_t for each value of the anisotropy parameter considered, we can plot the points at which the phase transition occurs, in terms of the quantities in equation 24, in order to obtain the phase diagram, as is shown in figure 9.

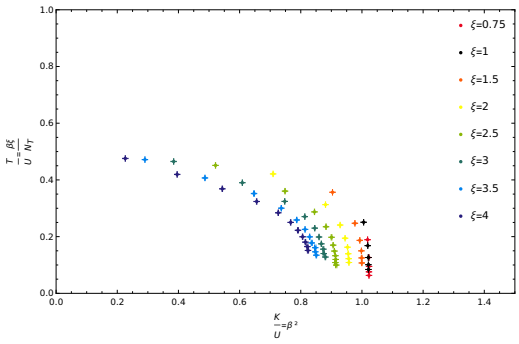

FIG. 9. Position of the peaks in the Polyakov loop susceptibility in terms of the quantities in equation 24

.

Plotting the coordinates of the phase transition in terms of the quantities in equation 24 is not enough to retrieve the phase diagram of the U(1) LGT. As can be seen in figure 9, the points for the position of the peaks in the Polyakov loop susceptibility do not line up in a single curve. This may happen because of the approximations used when deriving the action in equation 12 from the Hamiltonian model. In fact, if we are studying this theory outside of the region of validity of these approximations, the coefficient multiplying the space-time plaquette in the action, $1/\Delta\tau U$, may be incorrect, and it is thus not appropriate to use the parameterization in equation 24 to plot the phase diagram. In the following sections, we will explore this possibility, in order to obtain the correct phase diagram for this theory.

Correction to the Villain approximation: In order to retrieve the phase diagram of the $U(1)$ LGT we can consider a better approximation of the action from the Hamiltonian model, in equation 12. In section II, we derived the action in equation 10 from the Hamiltonian and further simplified the last two terms of this equation by using the Villain approximation, given by equation 11 [5] with $z = \frac{1}{\Delta\tau U}$. However, this approximation is valid only in the limit of large z [21]. Without considering this limit, the approximation can be expressed as

$$e^{z\cos(\Phi)} = \sum_n I_n(z) e^{in\Phi} \simeq \sum_n e^{-\frac{1}{2z_V}n^2 + i\Phi n} , \tag{25}$$

with $z_V = -\frac{1}{2\log\left(\frac{I_1(z)}{I_0(z)}\right)}$. In the limit $z \to \infty$, we have $z_V \approx z$ and we recover equation 11. Using now the approximation in equation 25 in the action in equation 10 with $z_V = \frac{1}{\Delta\tau U}$ we obtain

$$S[\phi] = -\Delta\tau K \sum_{n,\mu<\nu} \cos\left[\phi_\mu(n) + \phi_\nu(n+\hat{\mu}) - \phi_\mu(n+\hat{\nu}) - \phi_\nu(n)\right] - z\sum_{n,\mu} \cos\left[\phi_\mu(n) + \phi_0(n+\hat{\mu}) - \phi_\mu(n+e_0) - \phi_0(n)\right], \tag{26}$$

with z such that $\frac{1}{\Delta\tau U} = -\frac{1}{2\log\left(\frac{I_1(z)}{I_0(z)}\right)}$. By matching the coefficients multiplying the spatial and space-time parts of the action in equation 26 with the ones on the simulated action, in equation 14, along with the definition of the temperature, we obtain the relations

$$\frac{K}{U} = -\frac{\beta}{\xi}\frac{1}{2\log\left(\frac{I_1(\beta\xi)}{I_0(\beta\xi)}\right)} \quad , \quad \frac{T}{U} = -\frac{1}{N_t}\frac{1}{2\log\left(\frac{I_1(\beta\xi)}{I_0(\beta\xi)}\right)}. \tag{27}$$

We can now plot the critical points at which the phase transition occurs for each value of N_t and ξ in terms of the quantities defined in equation 27 and obtain the phase diagram shown in figure 10.

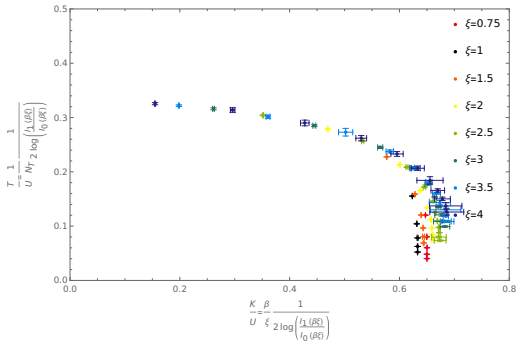

FIG. 10. Phase diagram using the relations in equation 27.

With this approach, we obtain a better collapsed phase diagram than in the initial case, in which we considered the action in equation 12. However, considering this correction on the Villain approximation does not fully collapse the phase diagram, in particular for larger values of $\frac{K}{U}$, which indicates that, although this approximation is more general than the one used when initially deriving the action from the Hamiltonian model, it is still not exact, and considering higher order approximations could provide further improvements on the collapse of the points for different values of ξ.

Rescaling of the phase diagram: The discussion in the previous sections makes it clear that the coefficient multiplying the space-time part of the action in equation 12 is not exact because of the approximations used to derive this action from the Hamiltonian in section II. Considering the next order Villain approximation in the previous section did not fully collapse the phase diagram which indicates that higher order approximations might be necessary. As such, in order to obtain the correct form of the phase diagram, we replace the coefficient multiplying the space-time part of the action with an unknown function of itself, and write the action as

$$S[\phi] = -\Delta\tau K \sum_{n,\mu<\nu} \cos\left[\phi_\mu(n) + \phi_\nu(n+\hat{\mu}) - \phi_\mu(n+\hat{\nu}) - \phi_\nu(n)\right] - f\left(\frac{1}{\Delta\tau U}\right)\sum_{n,\mu} \cos\left[\phi_\mu(n) + \phi_0(n+\hat{\mu}) - \phi_\mu(n+e_0) - \phi_0(n)\right]. \tag{28}$$

Again, by matching the coefficients multiplying each part of the previous action with the ones on the action in equation 14, we find the following relations

$$\frac{K}{U} = \frac{\beta\cdot g\left(\beta\xi\right)}{\xi} \quad , \quad \frac{T}{U} = \frac{g\left(\beta\xi\right)}{N_t}, \tag{29}$$

where we denote the inverse function of $f(x)$ by $g(x) = f^{-1}(x)$.

In order to find the form of the function $g(x)$ we set the condition that in the limit of zero temperature ($N_t \to +\infty$), the value of $\frac{K}{U}$ goes to 1, i.e., $\frac{K_0}{U} = 1$. Then, using the relations in equation 29, we find

$$\frac{K_0}{U} = 1 \Leftrightarrow \frac{\beta_0(\xi)\cdot g\left(\beta_0(\xi)\cdot\xi\right)}{\xi} = 1 \Leftrightarrow g\left(\beta_0(\xi)\cdot\xi\right) = \frac{\xi}{\beta_0(\xi)}, \tag{30}$$

where $\beta_0(\xi) = \lim_{N_t\to+\infty}\beta(N_t,\xi)$

Using the data obtained in the simulations, we can obtain the value of β_0 for each ξ. Then, by plotting $g(x) = \frac{\xi}{\beta_0}$ with respect to $x = \xi\cdot\beta_0(\xi)$, and performing a fit, we can find $g(x)$. We used a fit function of the form $g(x) = a + b\cdot x + c\cdot x^2 + d\cdot x^3 + e\cdot x^4$ and, with the expression found, we could obtain the phase diagram in equation 11 in terms of $\frac{K}{U}$ and $\frac{T}{U}$, defined in equation 29. Unlike in the initial case, in which the parameterization of the phase diagram was derived from the action in equation 12, here the data for different values of the anisotropy parameter ξ are collapsed in a single curve, showing the correct form of the phase diagram. This shows that indeed the term multiplying the space-time plaquette in the initial action was imprecise in the region we are working on, and scaling it with a function as in the action shown in equation 28 accounted for this fact.

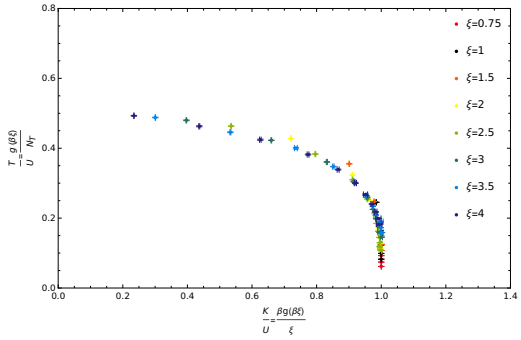

FIG. 11. Phase diagram using the parameters in equation 29.

Running coupling constant: In this section, we study the change of the coupling parameter, β, as we consider anisotropy, through the introduction of the anisotropy parameter, ξ in the lattice action. In order to do so, we will begin by briefly visiting the results of the running coupling constant for SU(N), and then propose an approach for the U(1) LGT.

In SU(N), the lattice gauge action can be written as[2]

$$S = \frac{\beta}{N}\sum_n\sum_{\mu<\nu} \mathrm{Re\,tr}\left[\mathbb{1} - U_{\mu\nu}(n)\right]. \tag{31}$$

Observables computed on the lattice depend on the lattice spacing a and on the bare coupling g. However, when taking the limit $a \to 0$, the lattice cutoff is removed, and, as such, physical observables must be independent of a. This implies that the bare coupling g must depend on a, so that the physical observables become independent on a as we take the limit $a \to 0$.

If $P(g(a),a)$ is a physical observable that reproduces the physical value on the limit $a \to 0$, this requirement is given by the differential equation

$$\frac{dP(g,a)}{d\ln a} = 0 \quad \Leftrightarrow \quad \left(\frac{\partial}{\partial \ln a} + \frac{\partial g}{\partial \ln a}\frac{\partial}{\partial g}\right) P(g,a) = 0\,. \tag{32}$$

The coefficient on the second term is the β-function, which gives the dependence of the coupling g on the lattice spacing a, $\beta(g) = \frac{\partial g}{\partial \ln a}$. This function can be expanded around $g = 0$ using perturbation theory and, in SU(N) is given by [22] $\beta(g) = -b_0 g^3 - b_1 g^5 + \mathcal{O}\left(g^7\right)$ with $b_0 = \frac{11N}{48\pi^2}$ and $b_1 = \frac{34}{3}\left(\frac{N}{16\pi^2}\right)^2$. Using this expression for the β-function, we can solve the differential equation given by $\beta(g) = \frac{\partial g}{\partial \ln a}$, which yields the relation between the lattice spacing a and the gauge coupling g. [23]

Considering the anisotropic lattice regularization, the action for SU(N), can be written as

$$S = \frac{\beta_t}{N}\sum_{n,\mu} \mathrm{Re\,tr}\left[\mathbb{1} - \Pi_{\mu 0}(n)\right] + \frac{\beta_s}{N}\sum_{n,\mu<\nu} \mathrm{Re\,tr}\left[\mathbb{1} - \Pi_{\mu\nu}(n)\right]\,, \tag{33}$$

with $\beta_t = \xi^2\beta_s$, where ξ is the anisotropy parameter. In the this case, the dependence of the lattice spacing on the coupling changes for each ξ.[22]

If we define $\frac{2N}{g_t^2} = \beta_t$ and $\frac{2N}{g_s^2} = \beta_s$ such that we can write $\frac{1}{g'^2} = \frac{1}{g_t}\frac{1}{g_s}$, we can expand these quantities around $\xi = 1$ as $\frac{1}{g_t} = \frac{1}{g} + c_t(\xi) + O(g^2)$ and $\frac{1}{g_s} = \frac{1}{g} + c_s(\xi) + O(g^2)$. Using this expansion, we can relate the anisotropic coupling parameters β_t and β_s with the isotropic coupling parameter β as

$$\beta_t = \xi\left(\beta + 2Nc_t(\xi)\right) \quad \beta_s = \frac{\beta + 2Nc_s(\xi)}{\xi}\,. \tag{34}$$

Considering the $\frac{1}{\xi}$ expansion of the functions c_t and c_s as $2Nc_{t,s} \equiv \alpha^0_{t,s} + \frac{\alpha^1_{t,s}}{\xi} + \cdots$, we can express the relation between the isotropic and anisotropic couplings in equation 34 as

$$\beta_t = \left(\beta + \alpha_t^0\right)\xi + \alpha_t^1 \quad \beta_s = \left(\frac{\beta + \alpha_s^0}{\xi}\right) + \frac{\alpha_t^1}{\xi^2}\,. \tag{35}$$

As we saw in the previous section, the temperature of an isotropic lattice with a temporal extent N_t is the same as that of an anisotropic lattice with anisotropy parameter ξ and a temporal extent of ξN_t. This fact, together with the results from this section, shows that considering an isotropic lattice with coupling β and N_t points in the temporal direction is equivalent to considering an anisotropic lattice with $\beta_s = \xi^2\beta_t$ and ξN_t points on the temporal direction, with β_t and β_s defined as equation 35. Classically, the equivalence between the anisotropic and isotropic lattices would be given by $\beta_t = \beta\xi$ and $\beta_s = \frac{\beta}{\xi}$, but in order to take into account the effects of quantum fluctuations at one loop, we must change the coupling parameters according to equation 35 [23].

The coefficients of the $\frac{1}{\xi}$ expansion of the functions $c_{t,s}$ have been determined for SU(N) by constructing an effective action for the LGT in terms of the Polyakov loop and taking its continuum limit, $a \to 0$. Since in this limit, the results should be independent of the regularization used, equating the actions for $\xi = 1$ and $\xi \neq 1$ gives the correct form of the functions $c_{t,s}$, and thus determines the running of the coupling parameters $\beta_{t,s}$ with the anisotropy parameter [23].

Running coupling in U(1) LGT: The form of the functions $c_{t,s}$ determining the change of the coupling parameter, β with the anisotropy parameter, ξ in U(1) LGT is not known. In order to find the ξ dependence of the coupling parameter, β, for anisotropic lattices, we can compare the values for the critical coupling at the phase transition obtained for lattices at constant values of ξN_t for several values of ξ. By plotting this data with respect to ξ and fitting a function through the points, we can obtain the functions $c_{t,s}$ determining the change of the coupling parameter with ξ. Starting from the form of the expression of the running coupling for SU(N) in equation 35 and adding terms of higher order in ξ, we propose an anzatz of the form $\beta_t = \left(\beta + \alpha_t^0\right)\xi + \alpha_t^1 + \alpha_t^2\xi^2 + \alpha_t^3\xi^3$, where β is the coupling parameter in the isotropic lattice with the temperature considered. Using this anzatz, we performed a fit with the data obtained for lattice regularizations with $\xi N_t = 4$, 6 and 8. Having determined the coefficients of the relation between the coupling parameter, β_t and the anisotropy parameter, ξ, we can now invert this function, and properly relate the results on the anisotropic lattice with the isotropic case, by changing $\beta_{t,c}$ as

$$\beta_{c,t}(\xi) \to \frac{\beta_{c,t}(\xi) - \alpha_t^1 - \alpha_t^2\xi^2 - \alpha_t^3\xi^3}{\xi} - \alpha_t^0\,. \tag{36}$$

By applying this transformation on the quantities $\frac{K}{U}$ and $\frac{T}{U}$, in equation 24 in respect to which we want to plot the phase diagram of the U(1) LGT we obtain the phase diagram shown in figure 12 using the fitting parameters obtained for lattice regularizations with $\xi N_t = 6$.

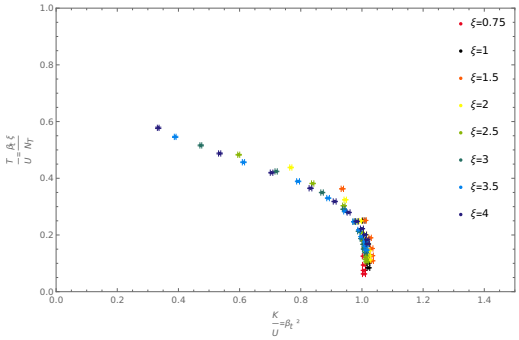

FIG. 12. Phase diagram of the U(1) LGT in terms of the parameters in equation 24 with the coupling parameter transformed according to equation 36, with the parameters obtained for lattice regularizations with $\xi N_t = 6$

Renormalized anisotropy parameter: By taking the continuum limit of the action for the U(1) LGT, we find, at the classical level, $\xi = \frac{a_s}{a_t}$. However, ξ is not the physical ratio between lattice spacings in the spatial and temporal directions, and we should refer to this parameter as the *bare anisotropy parameter*. The actual physical ratio between a_s and a_t can differ from the bare anisotropy parameter. In this section, we will look at a method to determine the *renormalized coupling parameter*, $\xi_r = \left(\frac{a_s}{a_t}\right)_{phys}$.

As we saw in section II, we can relate the potential between two static charges with the average value of the Wilson loop, $W_{st}(r,t)$, with r and t in lattice units. From equation 16, we see that we can determine the potential as

$$a_t V_t(r) = \log\left[\frac{W_{st}(r,t)}{W_{st}(r,t+1)}\right]\,, \tag{37}$$

which is valid at large temporal distances t.

If we consider a quantity similar to the Wilson loop, composed by Wilson lines in one spatial direction, but with the temporal propagators replaced by *spatial propagators* in another direction, we can define a *spatial Wilson loop*,

$W_{ss}(r_1, r_2)$, and relate it to the potential of a fermion-antifermion pair propagating in the spatial direction of the spatial propagator. This way, we can determine the spatial potential as

$$a_s V_s(r_1) = \log\left[\frac{W_{ss}(r_1, r_2)}{W_{ss}(r_1, r_2 + 1)}\right] . \tag{38}$$

The potentials $V_t(r)$ and $V_s(r)$ are measured, respectively, in units of a_t and a_s. As such, they differ by a factor of $\xi_r = \left(\frac{a_s}{a_t}\right)$. They should also differ by an additive constant, resulting from the fact that the self-energy corrections to the potential are different for spatial and temporal propagation [24]. As such, we have $a_s V_s(r) = \xi_r a_t V_t(r) + const.$ Therefore, we can compute the physical ratio between the spatial and temporal lattice spacings, by determining the spatial and temporal potentials, and calculating the ratio [24, 25]

$$\xi_r = \frac{a_s V_s(r_1) - a_s V_s(r_2)}{a_t V_t(r_1) - a_t V_t(r_2)} , \tag{39}$$

for two different distances r_1 and r_2, in lattice units.

The spatial and temporal potentials calculated with the Wilson loop at the phase transition are plotted in figure 13 for some values of the bare anisotropy parameter ξ. As expected, for the isotropic case with $\xi = 1$, the two potentials are the same as in this case there is no difference between the temporal and spatial directions. For $\xi = 0.75$, we find a temporal potential larger than the spatial potential, which is consistent with a value of ξ_r below 1. Consistently, for $\xi = 2$, we find a spatial potential larger then the temporal potential which is in accordance with a value of ξ_r greater than one. The errors in the potential increase rapidly with increasing distance r. This is due to the fact that the signal to noise ratio for the Wilson loop is very low, and decreases for large values of r.

In table I, we present the values of the physical ratio a_s/a_t calculated at the phase transition for the different values of ξ used. In the isotropic case, with $\xi = 1$, the values of the physical ratio between the lattice spacings are consistent with $\xi_r = 1$, as expected. For the anisotropic lattices considered, we can see that the value of ξ_r is greater that ξ for lattices with $\xi > 1$ and less that the value of ξ for the case with an anisotropy parameter $\xi < 1$, with the difference between the anisotropy parameter and the renormalised anisotropy parameter increasing with increasing ξ.

ξ	β	a_s/a_t		
		$R_1 = a_s$ $R_2 = 2a_s$	$R_1 = a_s$ $R_2 = 3a_s$	$R_1 = 2a_s$ $R_2 = 3a_s$
0.75	1.01145	0.545 ± 0.004	0.548 ± 0.014	0.55 ± 0.04
1	1.01057	1.00 ± 0.04	1.05 ± 0.05	1.19 ± 0.24
1.5	0.9998	1.78 ± 0.04	1.87 ± 0.11	2.00 ± 0.30
2	0.9785	2.46 ± 0.08	2.38 ± 0.09	2.26 ± 0.25
2.5	0.9570	3.19 ± 0.13	3.30 ± 0.15	3.5 ± 0.6
3	0.9383	3.89 ± 0.17	3.88 ± 0.22	3.9 ± 0.7
3.5	0.9223	4.42 ± 0.24	4.43 ± 0.29	4.5 ± 0.9
4	0.9075	5.00 ± 0.23	5.3 ± 0.4	5.7 ± 1.0

TABLE I. Values of $\left(\frac{a_s}{a_t}\right)_{phys}$ calculated at the phase transition on a 24^4 lattice, for each ξ, using different distances.

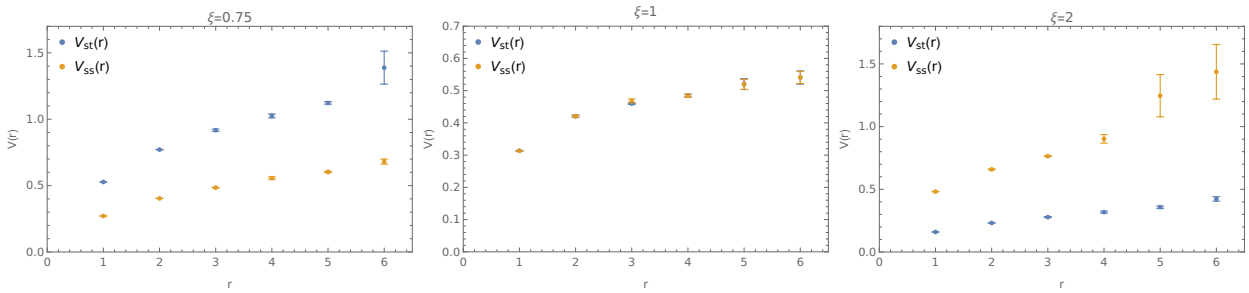

FIG. 13. Potential calculated on a 24^4 lattice for β at the phase transition, using the Wilson Loop, for several values of ξ.

VI. CONCLUSION

This project was motivated by the fact that, although many properties of the U(1) LGT have already been studied, a complete phase diagram for this theory was missing from the literature. In this work, by simulating the U(1) LGT on lattices with different sizes in the temporal and spatial directions using Markov Chain Monte Carlo methods, we were able to retrieve the full phase diagram of this theory.

For the isotropic lattice considered in the beginning of this work, we were able to identify the phase transition by looking at the Polyakov loop and the string tension as order parameters, and recover results consistent with those found in the literature. Then, by introducing anisotropy between the spatial and temporal directions on the lattice, we were able to probe the theory at higher temperatures, and thus obtain the coordinates of the phase transition in a broader parameter region. We were able to identify the order of the phase transition for different values of the lattice temporal extent for the isotropic regularization, determining that it is of first order at low temperatures, as defined in the Hamiltonian picture, and becomes weaker with increasing temperature until it becomes second order. However, this is not enough to identify the exact point where the order of the phase transition changes along the curve in the phase diagram. By considering anisotropic lattices, we were able to extend the range of temperatures and coupling parameters at which we were able to study the U(1) LGT. Therefore, in the future, in order to determine the value of the temperature at which the phase transition goes from discontinuous to continuous more accurately, it would be interesting to consider the anisotropic lattice regularization, and repeat the process used in section V to determine the order of the phase transition at different lattice extents in the temporal direction.

[1] K. G. Wilson, Phys. Rev. D **10**, 2445 (1974).
[2] C. Gattringer and C. B. Lang, *Quantum chromodynamics on the lattice*, Vol. 788 (Springer, Berlin, 2010).
[3] J. Smit, *Introduction to Quantum Fields on a Lattice (Cambridge Lecture Notes in Physics, 15)* (2002) pp. 1–284.
[4] J. Kogut and L. Susskind, Physical Review D **11**, 395 (1975).
[5] J. Villain, Journal de Physique **36**, 581 (1975).
[6] J. Engels, F. Karsch, H. Satz, and I. Montvay, Nuclear Physics B **205**, 545 (1982).
[7] A. M. Polyakov, *Gauge Fields and Strings*, Vol. 3 (1987).
[8] P. A. M. Dirac, Proceedings of the Royal Society of London. Series A, Containing Papers of a Mathematical and Physical Character **133**, 60 (1931).
[9] J. Gervais, A. Neveu, R. Jackiw, A. Jevicki, J. Kogut, T. Lee, S. Mandelstam, Y. Nambu, B. Sakita, B. Schroer, *et al.*, Non-linear and Collective Phenomena in Quantum Physics: A Reprint Volume from Physics Reports **23**, 6 (1983).
[10] A. M. Polyakov, Physics Letters B **59**, 82 (1975).
[11] T. Banks, R. Myerson, and J. Kogut, Nuclear Physics B **129**, 493 (1977).
[12] S. D. Drell, H. R. Quinn, B. Svetitsky, and M. Weinstein, Phys. Rev. D **19**, 619 (1979).
[13] N. Metropolis, A. W. Rosenbluth, M. N. Rosenbluth, A. H. Teller, and E. Teller, The Journal of Chemical Physics **21**, 1087 (1953).
[14] W. K. Hastings, Biometrika **57**, 97 (1970).
[15] D. P. Landau, *A guide to Monte Carlo simulations in statistical physics*, third edition. ed. (2013).
[16] M. Vettorazzo and P. De Forcrand, *Finite temperature phase transition in the 4d compact U(1) lattice gauge theory*, Tech. Rep. (2004).
[17] G. Parisi, R. Petronzio, and F. Rapuano, Phys. Lett. B **128**, 418 (1983).
[18] A. Irback and C. Peterson, Phys. Rev. D **36**, 3804 (1987).
[19] M. Lüscher and P. Weisz, Journal of High Energy Physics **2001**, 010–010 (2001).
[20] C. Bonati and M. D'elia, *Phase diagram of the 4D U(1) model at finite temperature*, Tech. Rep. (2013) arXiv:1305.3564v2.
[21] W. Janke and H. Kleinert, Nuclear Physics, Section B **270**, 135 (1986).
[22] F. Karsch, Nuclear Physics B **205**, 285 (1982).
[23] M. Billó, M. Caselle, A. D'Adda, and S. Panzeri, Nuclear Physics B **472**, 163 (1996), arXiv:9601020 [hep-lat].
[24] T. R. Klassen, Nucl. Phys. B **533**, 557 (1998), arXiv:hep-lat/9803010.
[25] N. H. Shakespeare and H. D. Trottier, Phys. Rev. D **59**, 014502 (1999), arXiv:hep-lat/9803024.